Chemical Communications RSCPublishing

COMMUNICATION

Engineered co-sensitization system for highly efficient dye solar cells†

Cite this: DOI: 10.1039/x0xx00000x

R. Agosta,[a‡] R. Grisorio,[b‡] L. De Marco,[a*] G. Romanazzi,[b] G. P. Suranna,[b*] G. Gigli[a,c,d] and M. Manca[a]

Received 00th January 2012,
Accepted 00th January 2012

DOI: 10.1039/x0xx00000x

www.rsc.org/

Novel co-sensitizers have been structurally tailored and implemented in a multi-sensitized devices demonstrating a synergic efficiency enhancement attributable to improved light-harvesting as well as prevention of charge recombination.

Dye-sensitized solar cells (DSSC) still represent to date the most suited candidate for the next generation of building integrated photovoltaics because of their peculiarity in terms of transparency and coloration which paves the way to novel applications. Aiming at improving the DSSC performances, substantial efforts have been devoted to the search for new and efficient fully-organic dyes, providing advantages in terms of the molecular design flexibility and higher molar extinction coefficients with respect to their inorganic counterparts.[1-3] In order to overcome the light-harvesting limits of organic sensitizers due to their narrower absorption bands, co-sensitization (employing multiple dyes with complementary absorption features) has recently emerged as a cunning approach to achieve a panchromatic optical response. It has already been shown that the co-deposition of two or more dyes lead to an improvement of the power conversion efficiency with respect to that attainable by the individual sensitizers.[4] At the same time, however, apart from a broadly extended absorption spectrum, the structure of an optimal sensitizer should also prevent recombination effects due to aggregation or stacking when absorbed onto the inorganic semiconductor surface. If this criterion is not met, the co-adsorption of an additive is again an appropriate remedy. An additive performs its favourable task by *i)* occupying the voids between the dye molecules, thus reducing charge recombination effects and by *ii)* assisting their packing on the TiO_2 surface avoiding aggregation. The examples of co-sensitization reported thus far have concentrated on the choice of the suitable co-adsorbents for the use in mixture with well-known high-performing dyes (porphyrins,[5] Ru-based complexes[6] or organic sensitizers[7]) without any evident structural correlation between the main sensitizer and the relevant co-adsorbent.

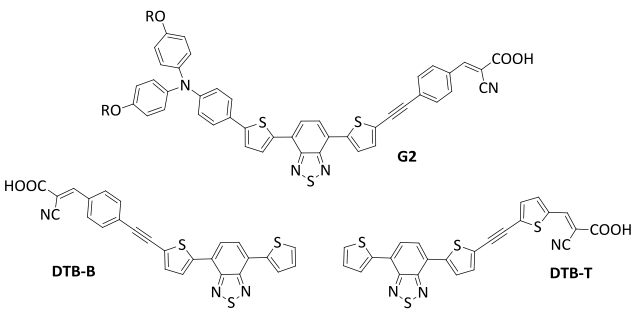

Fig. 1 Chemical structures of the main sensitizer **G2** and co-adsorbent **DTB-B** and **DTB-T** (R = 2-ethyl-hexyl).

In this work, we aim at demonstrating that the DSSC performances of largely π-extended sensitizers can be noticeably improved by co-deposition with a structurally analogous dye, providing a guideline for the selection of the dyes pair for suitable co-sensitization.

In the framework of our studies on novel organic dyes for DSSCs, we have recently embarked in the synthesis of **G2**[8] (Fig. 1), a sensitizer which was devised with an unusually extended benzothiadiazole-based π-bridge. The UV-vis spectrum of **G2**, as commonly observed for benzothiadiazole-based dyes,[9] is characterized by a "camelback" profile (Fig. 2), which leads to an absorption lacuna between 400 and 500 nm. Corroborated by DFT calculations and taking **G2** as starting structure, we have designed the co-sensitizers **DTB-B** and **DTB-T** (Fig. 1), that were endowed with *i*) a good absorption between 400 and 500 nm; *ii*) a suitable size to improve their co-deposition on the semiconductor surface; *iii*) conformational prerogatives to hamper molecular aggregation during the co-deposition. Removing the triarylamine donor from the structure of **G2** seemed as the simplest strategy to suitably increase the energy-gap of the relevant structures consequent to a remarkable lowering of the theoretical HOMO energy level of **DTB-B** and **DTB-T** with respect to **G2** without remarkably affecting their LUMO energy level (see Fig.S1). The calculated HOMO and LUMO levels guarantee the feasibility of the charge transfer

processes in the DSSC device and hint complementary absorption spectra with respect to that of **G2** as can clearly be evidenced comparing their simulated absorption spectra in Fig. S2. Owing to the presence of ethynylene moiety, the optimized geometry of **DTB-B** and **DTB-T** was found to be near planar, potentially favouring its co-adsorption into the interstitial sites left by a bulkier sensitizer on TiO_2 (Fig. S3). Furthermore, although deprived of a formal electron-donating group, the photo-excitation dynamics (simulated by their natural transition orbitals, Fig. S4) allows to hypothesize a partial shift of the electron density towards the anchoring portion of the molecule consequent to the photo-excitation, thus favouring the electron transfer in the course of the DSSC work cycle. The synthesis of **DTB-B** and **DTB-T** was carried out as described in the ESI. The products have been synthesized and characterized by elemental analyses, NMR, HR-MS, IR and cyclic voltammetry. The main sensitizer **G2**, shows two absorption bands at 373 nm (ε = 23200 $M^{-1}cm^{-1}$) and 538 nm (ε = 20000 $M^{-1}cm^{-1}$), Notably, the synthesised co-sensitizers show their main absorption peak at 471 nm (ε = 17000 $M^{-1}cm^{-1}$, **DTB-B**) and 475 nm (ε = 14500 $M^{-1}cm^{-1}$**,** **DTB-T**) nicely falling (Fig. 2) between the two absorption band recorded for **G2**.

Next, the photovoltaic performances of the fully-organic multi-sensitizer systems have been investigated. To this purpose, DSSC devices were constructed from TiO_2 photo-anodes co-sensitized with appropriate mixtures of **G2** and either **DBT-B** or **DTB-T** comparing the results with those obtained from devices embodying each of the single sensitizers. After the suitable screening (see Table S1) of the blend composition, it was found that the best results for the co-adsorption are obtained with a **G2**/ **DBT-B** (**DTB-T**) molar ratio of 2/1. Table 1 summarizes the open-circuit voltage (V_{OC}), short-circuit photocurrent density (J_{SC}), fill factor (FF), and power conversion efficiency (η), extracted from the photocurrent density-voltage (J-V) curves of the most representative devices. The PCE of devices A, B and C (based on **G2**, **DTB-B** and **DTB-T**) were 5.58%, 1.10% and 1.80%, respectively, whereas the performances of the co-sensitized devices D and E (which correspond to **G2/DTB-B** and **G2/DTB-T** systems) resulted in a conspicuous enhancement of the performance (6.22% and 7.84%, respectively) with respect to device A. Since the V_{oc} and FF values are very similar in devices A, D and E, the increase is mainly due to the higher photocurrent in the co-sensitized devices (13.86 and 15.33 mA/cm^2 for devices D and E, respectively). The dye loading of devices (mole of absorbed dye *per* cm^2 of TiO_2,

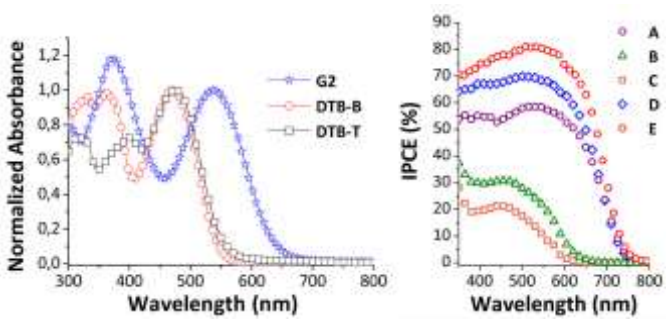

Fig. 2 (Left) Normalized absorption spectra of **G2**, **DTB-B** and **DTB-T** recorded in THF. (Right) IPCE spectra of devices A-E (see table 1).

Table 1 Photovoltaic parameters of devices based on individual dyes **DTB-B**, **DTB-T** and **G2** as well as co-sensitized devices measured under 1.0 sun illumination (AM 1.5, 100 mW/cm^2).

Device	Dye	J_{SC} [mA/cm^2]	V_{OC} [V]	FF	η [%]	Dye loading[b]
A	G2	11.39	0.70	0.70	5.58	2.1
B	DTB-B	2.86	0.54	0.71	1.10	3.4
C	DTB-T	4.02	0.58	0.77	1.80	3.2
D	G2/DTB-B[a]	13.86	0.67	0.67	6.22	1.7/1.3
E	G2/DTB-T[a]	15.33	0.71	0.72	7.84	1.8/1.5

[a]2/1 molar ratio; [b] [10^{-7} mol/cm^2].

Table 1) was estimated by UV-vis after dye desorption in alkaline solution (see ESI). The lower surface concentration of **G2** in device A (2.1 × 10^{-7} mol/cm^2) with respect to that of **DTB-B** and **DTB-T** dyes (3.4 × 10^{-7} and 3.2 × 10^{-7} mol/cm^2, in devices B and C, respectively) can be ascribed to the higher steric hindrance of the triarylamine containing **G2**. Dye desorption also allowed an estimate of the loading of individual dyes in co-sensitized photo-anodes D and E**.** A lower uptake for the individual sensitizers was estimated, however, the total dye loading was 3.0 × 10^{-7} and 3.3 × 10^{-7} mol/cm^2 for devices D and E, respectively, which is comparable to the result obtained for device B and C, suggesting that the TiO_2 surface coverage obtained with co-sensitization was complete. These results indicate that, when absorbed onto the titania surface, **G2** leaves enough space to allow the co-adsorption of the smaller and highly planar **DTB-B** or **DTB-T** dyes. The device characterization was completed by measuring the incident photon-to-current conversion efficiency (IPCE) spectra, shown in Fig. 2b. The photo-response of the **G2**-based device clearly evidences a drop at ~450 nm (corresponding to the absorption minimum recorded in the UV spectrum) which conversely could not be observed in the IPCE spectra of the co-sensitized devices D and E, due to the absorption of **DTB-B** and **DTB-T** dyes at ~450 nm. However, the sole light-harvesting effect is not sufficient to justify the above referred enhancement of the photocurrent density. The question is, therefore, shifted on the role of the dyes arrangement onto the TiO_2 surface in the increasing of the photovoltaic performances.

In order to experimentally address this issue, both electrochemical charge capacitance and charge transfer resistance at the TiO_2/dye/electrolyte interface have been measured for all devices by electrochemical impedance spectroscopy (EIS).[10] Figure 3 shows the measured capacitance (C_{meas}) and the charge transfer resistance (R_{CT}) as a function of corrected voltage. Consistently with the recorded photocurrent density values, the highest C_{meas} (indicating the amount of photo-generated electrons injected in TiO_2 conduction band) was observed for devices D and E, confirming the advantages brought about by the co-sensitization process. This result can be justified by admitting a combined effect of the reduced dye aggregation due to the presence of the co-sensitizer as well as to its contribution to the enhanced light-harvesting. Charge-transfer resistance (Fig 3) was also affected by the nature of the sensitizers; the co-sensitized device E showed higher recombination resistance with respect to the devices A-C. In fact, the co-sensitization of **G2** with **DTB-T** resulted

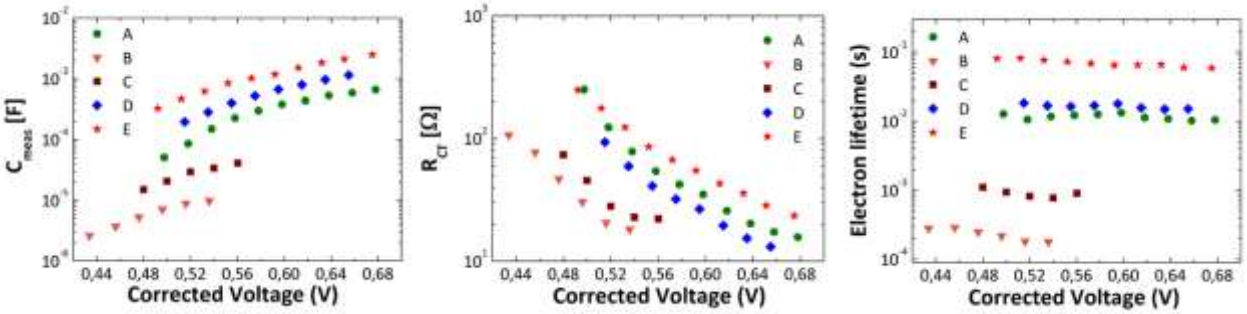

Fig. 3 Measured capacitance (left), charge transfer resistance (middle) and apparent electron lifetime (right) as a function of the corrected voltage for the devices A-E.

not only in an increase of injected electrons in the TiO_2 conduction band, but also in a drop in charge recombination at the TiO_2/electrolyte interface, as testified by the higher V_{OC} of device E. A different behaviour was observed for device D, which showed a lower R_{CT} value with respect to devices A and E, indicating that the **G2**/**DTB-B** co-sensitization is less efficient than the **G2**/**DTB-T** one in terms of recombination hindrance, in spite of its good photo-generated electrons injection ability. Eventually, the electron lifetime (τ_n) was calculated by the equation $\tau_n = R_{CT}C_{\mu}$.[11] The trend defined by the values of the electron lifetime, shown in Fig. 3, follows the one revealed by the photovoltaic measurements. The higher electron lifetime observed for device E demonstrates that the **G2**/**DTB-T** co-sensitization lead to an effective suppression of the recombination phenomena, probably due to the formation of a more compact dye layer uniformly covering the TiO_2 surface, thus reducing detrimental recombination between transferred electrons and triiodide acceptor.

In conclusion, we have developed a novel co-sensitization system which allows to simultaneously reduce the intermolecular quenching phenomena across the anchored dyes as well as to maximize the light harvesting capabilities of the photoelectrode. This unprecedented engineering of the co-adsorbents seems to induce a full synergy with the relevant main sensitizer, leading to photovoltaic performances higher than the sum of the corresponding individual component devices.

EFOR – Energia da Fonti Rinnovabili (Iniziativa CNR per il Mezzogiorno L. 191/2009 art. 2 comma 44); ESCORT-Efficient Solar Cells based on Organic and hybrid Technology (7th FWP—reference number 261920); DSSCX (MIUR-PRIN 2010-2011 No. 20104XET32); MAAT (MIUR – PON02_00563_3316357 – CUP B31C12001230005) and Daunia Wind are gratefully acknowledged for funding. The authors are indebted to Dr. R. Bisconti and Dr. R. Giannuzzi for beneficial discussions and to Dr. A. Cortese and D. Loliva for technical assistance.

Notes and references

[a]CBN, Center for Biomolecular Nanotechnologies, Fondazione Istituto Italiano di Tecnologia - Energy Platform Via Barsanti, 73010 Arnesano (Lecce), Italy. E-mail: luisa.demarco@iit.it
[b]DICATECh - Politecnico di Bari, Via Orabona, 4 I-70125 Bari, Italy. E-mail: surannag@poliba.it
[c]National Nanotechnology Laboratory (NNL), CNR Istituto Nanoscienze, c/o Distretto Tecnologico, Via Arnesano km 5, 73100 Lecce, Italy.
[d]Dipartimento di Matematica e Fisica "E. De Giorgi" - Università del Salento, via per Arnesano, 73100 Lecce, Italy.

† Electronic Supplementary Information (ESI) available: experimental details, DFT calculations, device fabrication and characterization. See DOI: 10.1039/c000000x/

‡ These authors equally contributed to the experimental work.

1 A. Hagfeldt, G. Boschloo, L. Sun, L. Kloo and H. Pettersson, *Chem. Rev.*, 2010, **35**, 6595.
2 S. K. Balasingam, M. Lee, M. G. Kang and Y. Jun, *Chem. Commun.*, 2013, **49**, 1471.
3 S. Zhang, X. Yang, Y. Numata and L. Han, *Energy Environ. Sci.*, 2013, **6**, 1443.
4 Y. Numata, S. Zhang, X. Yang and L. Han, *Chem. Lett.*, 2013, **42**, 1328.
5 (a) S. Chang, H. Wang, Y. Hua, Q. Li, X. Xiao, W.-K. Wong, W. Y. Wong, X. Zhu and T. Chen, *J. Mater. Chem. A*, 2013, **1**, 11553. (b) C.-M. Lan, H.P. Wu, T.-Y. Pan, C.-W. Chang, W.-S. Chao, C.-T. Chen, C.-L. Wang, C.-Y. Lin and E. W.-G. Diau, *Energy Environ. Sci.*, 2012, **5**, 6460. (c) M. Kimura, H. Nomoto, N. Masaki and S. Mori, *Angew. Chem. Int. Ed.* 2012, **51**, 4371. (d) H.-P. Wu, Z.-W. Ou, T.-Y. Pan, C.-M. Lan, W.-K. Huang, H.-W. Lee, N. M. Reddy, C.-T. Chen, W.-S. Chao, C.-Y. Yeh and E. W.-G. Diau, *Energy Environ. Sci.*, 2012, **5**, 9843. (e) A. Yella, H.-W. Lee, H. N. Tsao, C. Yi, A. K. Chandiran, M. K. Nazeeruddin, E. W.-G. Diau, C.-Y. Yeh, S. M. Zakeeruddin and M. Grätzel, *Science*, 2011, **334**, 629.
6 (a) S. Zhang, A. Islam, X. Yang, C. Qin, K. Zhang, Y. Numata, H. Chen and L. Han, *J. Mater. Chem. A*, 2013, **1**, 4812. (b) H. Ozawa, R. Shimizu and H. Arakawa, *RSC Advances*, 2012, **2**, 3198. (c) L. Han, A. Islam, H. Chen, C. Malapaka, B. Chiranjeevi, S. Zhang, X. Yang and M. Yanagida, *Energy Environ. Sci.*, 2012, **5**, 6057.
7 (a) R. Y.-Y. Lin, H.-W. Lin, Y.-S. Yen, C.-H. Chang, H.-H. Chou, P.-W. Chen, C.-Y. Hsu, Y.-C. Chen, J. T. Lin and K.-C. Ho, *Energy Environ. Sci.*, 2013, **6**, 2477. (b) M. Zhang, Y. Wang, M. Xu, W. Ma, R. Li and P. Wang, *Energy Environ. Sci.*, 2013, **6**, 2944. (c) M. Zhang, J. Zhang, Y. Fan, L. Yang, Y. Wang, R. Li and P. Wang, *Energy Environ. Sci.*, 2013, **6**, 2939. (d) I. T. Choi, M. J. Ju, S. H. Song, S. G. Kim, D. W. Cho, C. Im and H. K. Kim, *Chem. Eur. J.*, 2013, **19**, 15545. (e) J.-H. Yum, T. W. Holcombe, Y. Kim, J. Yoon, K. Rakstys, M. K. Nazeeruddin and M. Grätzel, *Chem. Commun.*, 2012, **48**, 10727. (f) J.-H. Yum, S. R. Jang, P. Walter, T. Geiger, F. Nuesch, S. Kim, J. Ko, M. Gratzel and M. K. Nazzeruddin, *Chem. Commun.*, 2007, **44**, 4680.
8 R. Grisorio, L. De Marco, R. Agosta, R. Iacobellis, M. Manca, P. Mastrorilli, G. Gigli and G. P. Suranna, *manuscript in preparation*.
9 (a) Y. Wu and W. Zhu, *Chem. Soc. Rev.*, 2013, **42**, 2039. (b) Y. Wu, M. Marszalek, S. M. Zakeeruddin, Q. Zhang, H. Tian, M. Gratzel, W. Zhu, *Energy Environ. Sci.*, 2012, **5**, 8261. (c) D. H. Lee, M. J. Lee, H. M. Song, B. J. Song, K. D. Seo, M. Pastore, C. Anselmi, S. Fantacci, F. De Angelis, M. K. Nazeeruddin, M. Gratzel, H. K. Kim, *Dyes Pigm.*, 2011, **91**, 192.
10 J. Bisquert, *J. Electroanal. Chem.*, 2010, **646**, 43.
11 J. Bisquert, F. Fabregat-Santiago, I. Mora-Sero', G. Garcia-Belmonte and S. Gimnez, *J. Phys. Chem.*, 2009, **113**, 17278.

COMMUNICATION

Electronic Supplementary Information for

Engineered co-sensitization system for highly efficient dye solar cells

by

R. Agosta, R. Grisorio, L. De Marco, G. Romanazzi, G. P. Suranna, G. Gigli and M. Manca

General remarks: all reactants were purchased from standard commercial sources and used without any further purification. All solvents used were carefully dried and freshly distilled according to standard laboratory practice. All manipulations were carried out under inert nitrogen atmosphere. Flash chromatography was performed using a silica gel of 230-400 mesh. ^{1}H and $^{13}C\{^{1}H\}$ NMR spectra were recorded on a Bruker Avance 700 MHz instrument. Melting points were measured on a Büchi B-545 instrument. Elemental analyses were obtained on a EuroVector CHNS EA3000 elemental analyser on the basis of three replicates. The high resolution electrospray ionization mass spectrometry (HR ESI-MS) analyses were performed using a Bruker microTOF QII mass spectrometer equipped with an electrospray ion source operated in positive ion mode. The sample solutions (CH_2Cl_2/MeOH) were introduced by continuous infusion at a flow rate of 180 μL/min with the aid of a syringe pump. The instrument was operated with end-plate offset and capillary voltages set to −500 V (500 V) and −4500 V (3500 V), respectively. The nebulizer pressure was 0.4 bar (N_2), and the drying gas (N_2) flow rate was 4.0 L/min. The capillary exit and skimmer 1 voltages were 90 V and 30 V, respectively. The drying gas temperature was set at 180°C. The calibration was carried out with sodium formate. FT-IR measurements were carried out on a JASCO FT/IR 4200 spectrophotometer. UV-Vis spectra were recorded on a Jasco V-670 instrument. Cyclic voltammetry was carried out on a Metrohm Autolab PGSTAT 302-N potentiostat. The materials were drop cast on a platinum working electrode from a 1 mg/mL THF (tetrahydrofuran) solution. Measurements were carried at 25 °C in acetonitrile solution containing tetrabutylammonium tetrafluoroborate (0.025 M) as supporting electrolyte with a scan rate of 50 mV/s. The potentials were measured versus Ag/Ag^+ as the quasi-reference electrode. After each experiment, the potential of the Ag/Ag^+ electrode was calibrated against the ferrocene/ferrocenium (Fc/Fc^+) redox couple. The electrochemical energy gap was determined as the difference between the onsets of the oxidation and the reduction potentials ($E_g^{elc} = E_{ox}^{onset} - E_{red}^{onset}$). The HOMO and LUMO energy values were estimated from the onset

potentials of the first oxidation and reduction event, respectively. After calibration of the measurements against Fc/Fc^+, the HOMO and LUMO energy levels were calculated according to the following equations:

E_{HOMO} (eV) = – [E_{ox}^{onset} – $E_{1/2}(Fc/Fc^+)$ + 4.8]

E_{LUMO} (eV) = – [E_{red}^{onset} – $E_{1/2}(Fc/Fc^+)$ + 4.8]

where $E_{1/2}(Fc/Fc^+)$ is the half-wave potential of the Fc/Fc^+ couple (the oxidation potential of which is assumed at 4.8 eV) against the Ag/Ag^+ electrode. The HOMO and LUMO levels evaluated for **DTB-B** and **DTB-T** were very similar (–5.4 eV and –3.4 eV, respectively) for both dyes. Density functional theory (DFT) and time-dependent DFT (TD-DFT) calculations were carried out with the Gaussian09 program package.

Synthesis of DTB-B and DTB-T

The synthetic sequence followed for the obtainment of **DTB-B** and **DTB-T** is illustrated in Scheme 1S. Reaction of 4,7-bis-thiophen-2-yl-benzo[2,1,3]thiadiazole with an equimolar amount of N-bromo-succinimide (NBS) allowed the obtainment of the corresponding mono-bromo derivative **2**. A Pd-catalyzed Sonogashira cross-coupling between **2** and trimethylsilyl-acetylene resulted in the functionalization with the ethynylene moiety, yielding the alkyne **3**. The trimethylsilyl protecting group in **3** could be easily removed by reaction with potassium fluoride affording the terminal alkyne **4**. At this stage of the synthetic procedure, the assembly of the □-bridges was completed by a further Sonogashira cross-coupling of **4** with either 4-bromobenzaldehyde or 5-bromo-thiophene-2-carbaldehyde to obtain aldehydes **5** and **6**, respectively. The synthesis was completed by introduction of the cyano-acrylic functionality by submitting **5** and **6** to a Knoevenagel condensation with cyanoacetic acid in the presence of ammonium acetate eventually yielding the target molecules **DTB-B** and **DTB-T**, respectively. The synthetic procedure is depicted in Scheme 1S and the characterization of the intermediates is described below.

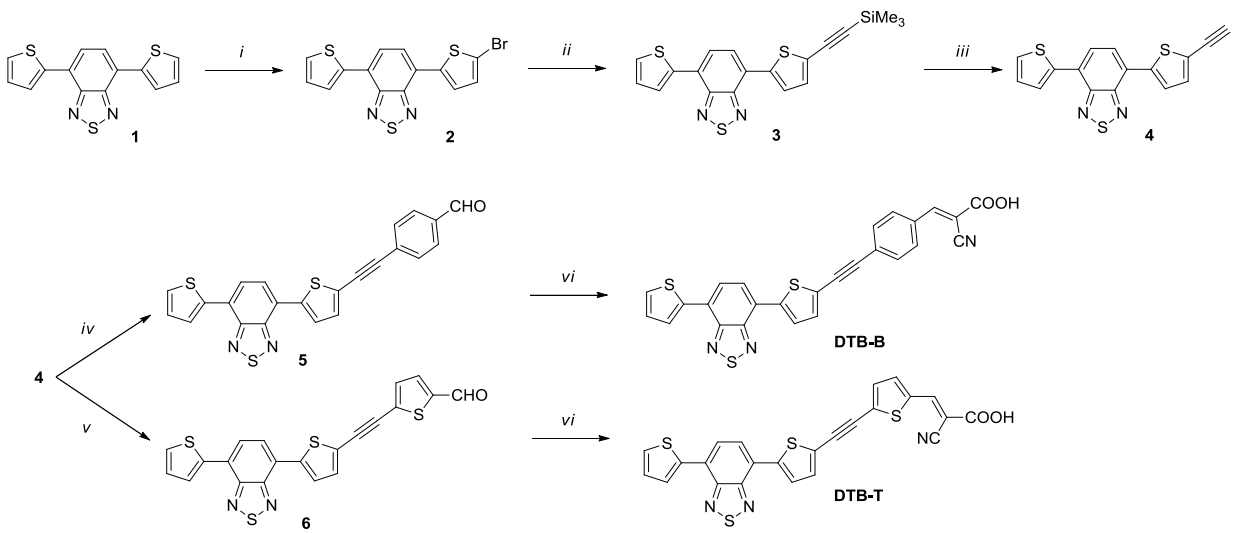

Scheme 1S. Synthetic approach for the obtainment of **DTB-B** and **DTB-T**.

4-(5-Bromo-thiophen-2-yl)-7-(thiophen-2-yl)-benzo[2,1,3]thiadiazole (2). A solution of N-bromo-succinimide (0.89 g, 5.00 mmol) in DMF (30 mL) was added dropwise to a solution of **1** (1.51 g, 5.00 mmol) in DMF (45 mL) kept at 0 °C. After the addition, the obtained reaction mixture was warmed to room temperature and allowed to react for further 2 h before quenching with water (50 mL). The products was extracted with diethyl ether (3 × 50 mL) and the combined organic phases were washed with brine and dried over Na_2SO_4. After solvent removal, the crude product was purified by column chromatography (SiO_2, petroleum ether 40-60 °C/CH_2Cl_2 = 4/1 v/v) and, subsequently, by crystallization with ethanol to afford **2** (0.65 g, 35%)

as a red solid. m. p.: 117.5±0.5 °C. ^{1}H NMR (700 MHz, $CDCl_3$): □8.11 (dd, J = 3.7, 1.1 Hz, 1H), 7.86-7.73 (m, 3H), 7.46 (dd, J = 5.0, 1.0 Hz, 1H), 7.20 (dd, J = 5.0, 3.9 Hz, 1H), 7.14 (d, J = 3.9 Hz, 1H) ppm. ^{13}C{^{1}H} NMR (176 MHz, $CDCl_3$): □152.6, 152.2, 140.8, 139.3, 130.8, 128.1, 127.6, 127.4, 126.9, 126.4, 125.8, 125.1, 125.0, 114.6 ppm. HR-MS (ESI) calcd for $C_{14}H_7BrN_2S_3Na$ $(M+Na)^+$: 402.8825 m/z; found: 402.8873 m/z. IR (KBr): □$_{max}$ 3090, 1481, 1423, 1215, 879, 833 cm^{-1}. Elem. Anal. calcd for $C_{14}H_7BrN_2S_3$: C, 44.33; H, 1.86, N, 7.39; found: C, 44.17; H, 1.86; N, 7.36.

4-(5-Trimethylsilylethynyl-thiophen-2-yl)-7-(thiophen-2-yl)-benzo[2,1,3]thiadiazole (3). A mixture of **2** (0.39 g, 1.02 mmol), $Pd(PPh_3)_4$ (58.9 mg, 5.1 × 10^{-2} mmol), CuI (9.7 mg, 5.1 × 10^{-2} mmol) and trimethylsilylacetylene (0.11 g, 1.12 mmol) in triethylamine (15 mL) was refluxed for 24 h under vigorous stirring. After cooling down the reaction mixture to room temperature, methylene chloride (50 mL) was added and the resulting organic phase was washed with water (50 mL) and dried over Na_2SO_4. Upon the solvent removal, the crude product was purified by column chromatography (SiO_2, petroleum ether 40-60 °C/CH_2Cl_2 = 4/1 v/v) to give **3** (0.36 g, 89%) as an orange solid. m. p.: 120.7±0.5 °C. ^{1}H NMR (700 MHz, $CDCl_3$): □8.10 (dd, J = 4.1, 1.1 Hz, 1H), 7.92 (d, J = 4.1 Hz, 1H), 7.84-7.79 (m, 2H), 7.46 (dd, J = 5.2, 1.1 Hz, 1H), 7.30 (d, J = 4.1 Hz, 1H), 7.20 (dd, J = 5.2, 4.1 Hz, 1H), 0.29 (s, 9H) ppm. ^{13}C{^{1}H} NMR (176 MHz, $CDCl_3$): □152.8, 152.7, 140.9, 139.5, 132.5, 132.4, 128.9, 128.8, 128.3, 127.8, 127.4, 126.8, 125.4, 124.7, 101.2, 98.0, 0.2 ppm. HR-MS (ESI) calcd for $C_{19}H_{16}N_2S_3SiNa$ $(M+Na)^+$: 419.0137 m/z; found: 419.0182 m/z. IR (KBr): □$_{max}$ 3078, 2952, 2920, 2849, 2138, 1482, 1247, 843, 801, 756, 683 cm^{-1}. Elem. Anal. calcd for $C_{19}H_{16}N_2S_3Si$: C, 57.54; H, 4.07; N, 7.06; found: C, 57.57; H, 4.10; N, 7.02.

4-(5-Ethynyl-thiophen-2-yl)-7-(thiophen-2-yl)-benzo[2,1,3]thiadiazole (4). A mixture of **3** (0.36 g, 0.90 mmol) and KF (0.26 g, 4.50 mmol) in methylene chloride (5 mL) and methanol (5 mL) was stirred for 30 min at 55 °C. After cooling down the reaction mixture to room temperature, methylene chloride (50 mL) was added and the resulting organic phase was washed with water (50 mL) and dried over Na_2SO_4. After solvent removal, the crude product was purified by column chromatography (SiO_2, petroleum ether 40-60 °C/CH_2Cl_2 = 4/1 v/v) yielding **4** (0.26 g, 88%) as an orange solid. m. p.: 136.3±0.5 °C. ^{1}H NMR (700 MHz, $CDCl_3$): □8.13 (dd, J = 4.1, 1.1 Hz, 1H), 7.95 (d, J = 4.1 Hz, 1H), 7.88- 7.84 (m, 2H), 7.47 (dd, J = 5.2, 1.1 Hz, 1H), 7.35 (d, J = 4.1 Hz, 1H), 7.21 (dd, J = 5.2, 4.1 Hz, 1H), 3.48 (s, 1H) ppm. ^{13}C{^{1}H} NMR (176 MHz, $CDCl_3$): □152.9, 152.8, 141.2, 139.5, 134.2, 128.4, 128.3, 128.1, 127.8, 127.5, 127.2, 127.0, 126.3, 126.1, 125.9, 125.4, 123.5, 83.3, 77.4 ppm. HR-MS (ESI) calcd for $C_{16}H_8N_2S_3Na$ $(M+Na)^+$: 346.9742 m/z; found: 346.9772 m/z. IR (KBr): □$_{max}$ 3080, 2922, 2851, 2089, 1484, 1213,

876, 830, 801, 786, 699, 661 cm^{-1}. Elem. Anal. calcd for $C_{16}H_8N_2S_3$: C, 59.23; H, 2.49; N, 8.63; found: C, 59.27; H, 2.50; N, 8.62.

4-((5-(7-(Thiophen-2-yl)-benzo[2,1,3]thiadiazol-4-yl)-thiophen-2-yl-ethynyl)-benzaldehyde (5). A mixture of **4** (0.12 g, 0.37 mmol), 4-bromo-benzaldeide (68.5 mg, 0.37 mmol), $Pd(PPh_3)_4$ (42.7 mg, 3.7×10^{-2} mmol) and CuI (7.1 mg, 3.7×10^{-2} mmol) in triethylamine (15 mL) was refluxed for 24 h under vigorous stirring. After cooling down the reaction mixture to room temperature, methylene chloride (50 mL) was added and the resulting organic phase was washed with water (50 mL) and dried over Na_2SO_4. After solvent removal, the crude product was purified by column chromatography (SiO_2, CH_2Cl_2) yielding **5** (64.3 mg, 41%) as a red solid. m. p.: 181.3±0.9 °C. ^{1}H-NMR (700 MHz, $CDCl_3$): □10.5 (s, 1H), 8.17 (dd, J = 3.9, 1.2 Hz, 1H), 8.05 (d, J = 3.9 Hz, 1H), 7.93-7.90 (m, 4H), 7.71 (d, J = 8.5 Hz, 2H), 7.51 (dd, J = 5.0, 1.2 Hz, 1H), 7.45 (d, J = 3.9 Hz, 1H), 7.25 (dd, J = 5.0, 3.9 Hz, 1H) ppm. $^{13}C\{^1H\}$ NMR (176 MHz, $CDCl_3$): □191.3, 152.6, 152.5, 141.8, 139.2, 135.5, 133.7, 131.8, 129.7, 129.2, 128.1, 127.9, 127.2, 127.2, 126.8, 126.0, 125.6, 125.0, 123.6 ppm. HR-MS (ESI) calcd for $C_{23}H_{12}N_2OS_3Na$ $(M+Na)^+$: 451.0004 m/z; found: 450.9965 m/z. IR (KBr): □$_{max}$ 3070, 2920, 2857, 2187, 1682, 1600, 1210, 818 cm^{-1}. Anal. calcd for $C_{23}H_{12}N_2OS_3$: C, 64.46; H, 2.82; N, 6.54; found: C, 64.44; H, 2.80; N, 6.53.

5-((5-(7-(Thiophen-2-yl)-benzo[2,1,3]thiadiazol-4-yl)-thiophen-2-yl-ethynyl)-thiophene-2-carbaldehyde (6). A mixture of **4** (0.13 g, 0.40 mmol), 5-bromo-thiophene-2-carbaldehyde (0.08 g, 0.44 mmol), $Pd(PPh_3)_4$ (46.2 g, 4.0×10^{-2} mmol) and CuI (7.6 mg, 4.0×10^{-2} mmol) in triethylamine (15 mL) was refluxed for 24 h under vigorous stirring. After cooling down the reaction mixture to room temperature, methylene chloride (50 mL) was added and the resulting organic phase was washed with water (50 mL) and dried over Na_2SO_4. After solvent removal, the crude product was purified by column chromatography (SiO_2, CH_2Cl_2) yielding **6** (95.6 mg, 55%) as a red solid. m. p.: 189.4±0.8 °C. ^{1}H NMR (700 MHz, $CDCl_3$): □ 9.90 (s, 1H), 8.17 (d, J = 3.5 Hz, 1H), 8.04 (d, J = 4.2 Hz, 1H), 7.92 (s, 2H), 7.71 (d, J = 3.5 Hz, 1H), 7.51 (d, J = 4.8 Hz, 1H), 7.45 (d, J = 4.2 Hz, 1H), 7.36 (d, J = 3.5 Hz, 1H), 7.26-7.24 (m, 1H) ppm. $^{13}C\{^1H\}$ NMR (176 MHz, $CDCl_3$): □182.3, 152.6, 152.5, 144.2, 142.4, 139.2, 136.0, 134.0, 132.5, 132.4, 128.2, 127.9, 127.3, 127.2, 126.9, 126.1, 125.6, 124.8, 122.8, 91.6, 87.5 ppm. HR-MS (ESI) calcd for $C_{21}H_{11}N_2OS_4$ $(M+H)^+$: 434.9749 m/z; found: 434.9676 m/z. IR (KBr): □$_{max}$ 3097, 2920, 2852, 2182, 1653, 1419, 1226, 834, 807 cm^{-1}. Anal. calcd for $C_{21}H_{10}N_2OS_4$: C, 58.04; H, 2.32; N, 6.45; found: C, 58.00; H, 2.29; N, 6.43.

2-Cyano-3-(4-((5-(7-(thiophen-2-yl)-benzo[2,1,3]thiadiazol-4-yl)-thiophen-2-yl)ethynyl)phenyl)-acrylic acid (DTB-B). A mixture of **5** (59.4 mg, 0.12 mmol),

cyano-acetic acid (0.10 g, 1.20 mmol) and ammonium acetate (9.2 mg, 0.12 mmol) in acetic acid (10 mL) was refluxed overnight. The mixture was allowed to reach room temperature and then poured into water (200 mL) to obtain a precipitate that was collected by filtration and washed with water. The crude product was purified by column chromatography (SiO_2, CH_2Cl_2/MeOH = 10/1 v/v) affording **DTB-B** (54.7 mg, 92%) as a red solid. ^{1}H NMR (700 MHz, DMSO-d_6): δ 8.42-8.01 (br, 8H), 7.85-7.73 (br, 2H), 7.64 (br, 1H), 7.30 (br, 1H) ppm. HR-MS (ESI) calcd for $C_{26}H_{12}N_3O_2S_3$ $(M–H)^–$: 494.0092 m/z; found: 494.0211 m/z. IR (KBr): ν_{max} 3097, 2921, 2226, 2183, 1696, 1573, 1427, 1181, 833 $cm^{–1}$. Anal. calcd for $C_{26}H_{13}N_3O_2S_3$: C, 63.01; H, 2.64; N, 8.48; found: C, 63.03; H, 2.63; N, 8.46.

2-Cyano-3-(5-((5-(7-(thiophen-2-yl)-benzo[2,1,3]thiadiazol-4-yl)-thiophen-2-yl)ethynyl)thiophen-2-yl)-acrylic acid (DTB-T). A mixture of **6** (73.9 mg, 0.17 mmol), cyano-acetic acid (0.14 g, 1.70 mmol) and ammonium acetate (13.1 mg, 0.17 mmol) in acetic acid (10 mL) was refluxed overnight. The mixture was allowed to reach room temperature and then poured into water (200 mL) to obtain a precipitate that was collected by filtration and washed with water. The crude product was purified by column chromatography (SiO_2, CH_2Cl_2/MeOH = 10/1 v/v) affording **DTB-T** (77.5 mg, 91%) as a red solid. ^{1}H NMR (700 MHz, DMSO-d_6): δ 8.30-8.13 (br, 5H), 8.00 (br, 1H), 7.81 (d, J = 4.5 Hz, 1H), 7.71-7.53 (br, 2H), 7.30-7.28 (br, 1H) ppm. HR-MS (ESI) calcd for $C_{24}H_{10}N_3O_2S_4$ $(M–H)^–$: 499.9656 m/z; found: 499.9448 m/z. IR (KBr): ν_{max} 3097, 2920, 2220, 2176, 1690, 1575, 1410, 1270, 1235, 806 $cm^{–1}$. Anal. calcd for $C_{24}H_{11}N_3O_2S_4$: C, 57.46; H, 2.21; N, 8.38; found: C, 57.43; H, 2.23; N, 8.41.

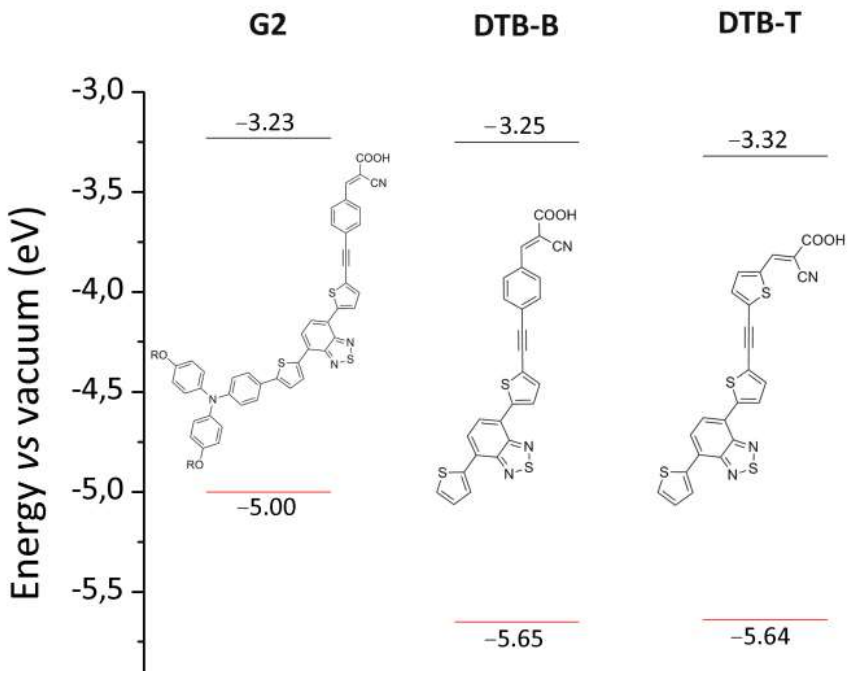

Figure S1. Theoretical HOMO (red) and LUMO (black) energy levels of the sensitizers **G2**, **DTB-B** and **DTB-T** calculated at the B3LYP/6-311G(d,p) level of the theory in THF (CPCM method). The relevant chemical structures are also shown (R = 2-ethyl-hexyl).

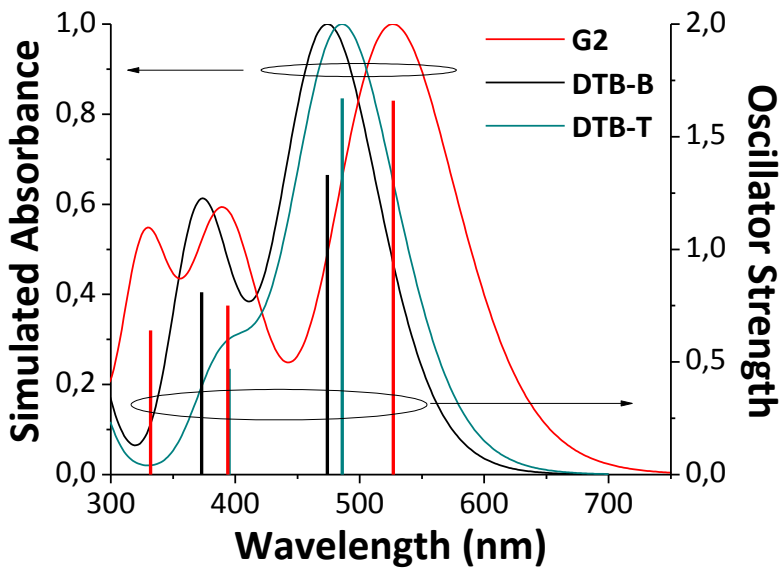

Figure S2. Simulated absorption spectra and oscillator strengths of **G2**, **DTB-B** and **DTB-T** calculated *in vacuo* at the CAM-B3LYP/6-31G(d,p) level of the theory.

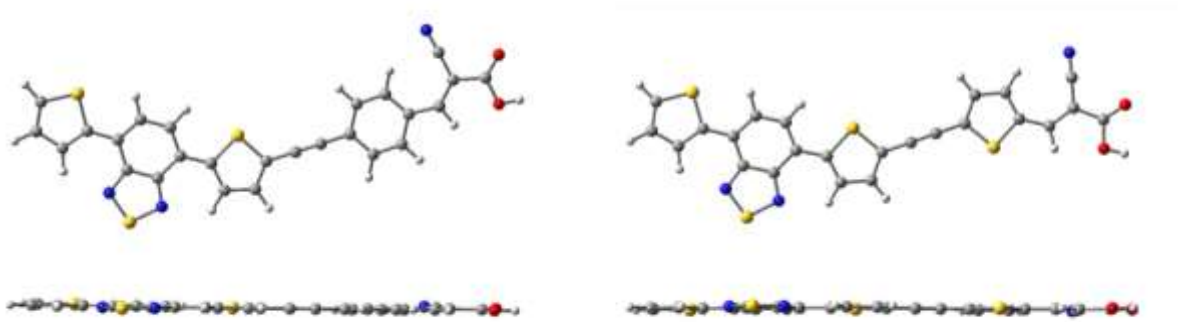

Figure 3S. Optimized molecular geometries of **DTB-B** (left) and **DTB-T** (right) calculated *in vacuo* at the B3LYP/6-31G(d,p) level of the theory.

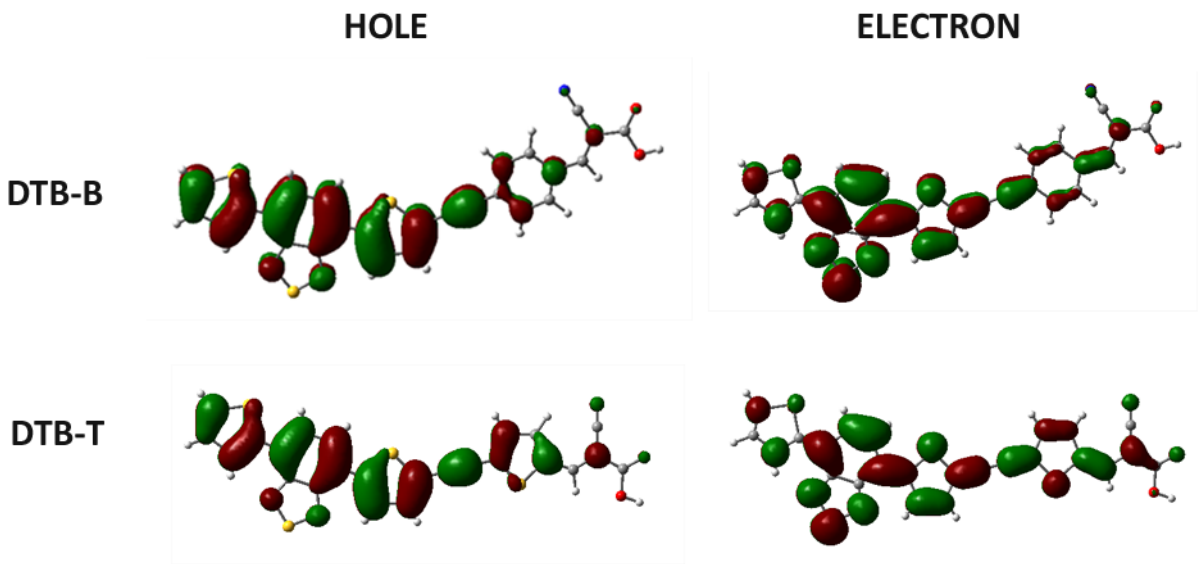

Figure 4S. Natural transition orbitals defining the photo-excitation dynamics of the main electronic transition in **DTB-B** and **DTB-T** calculated *in vacuo* at the CAM-B3LYP/6-31G(d,p) level of the theory.

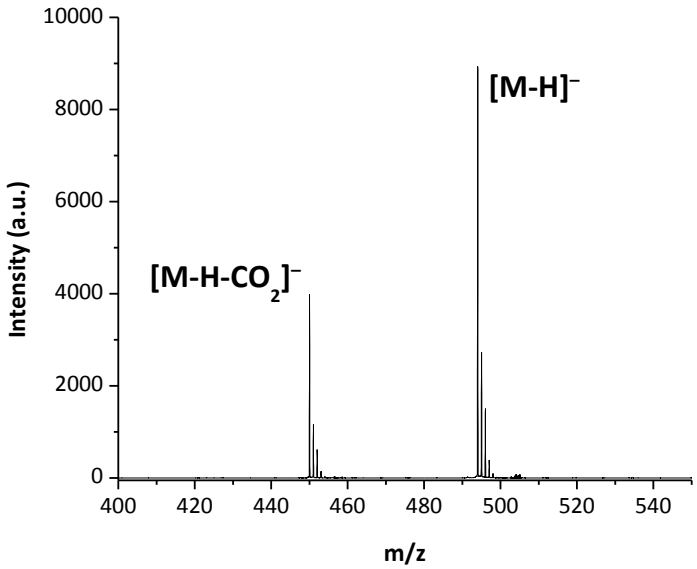

Figure 5S. HR-MS (ESI) spectrogram of **DTB-B**.

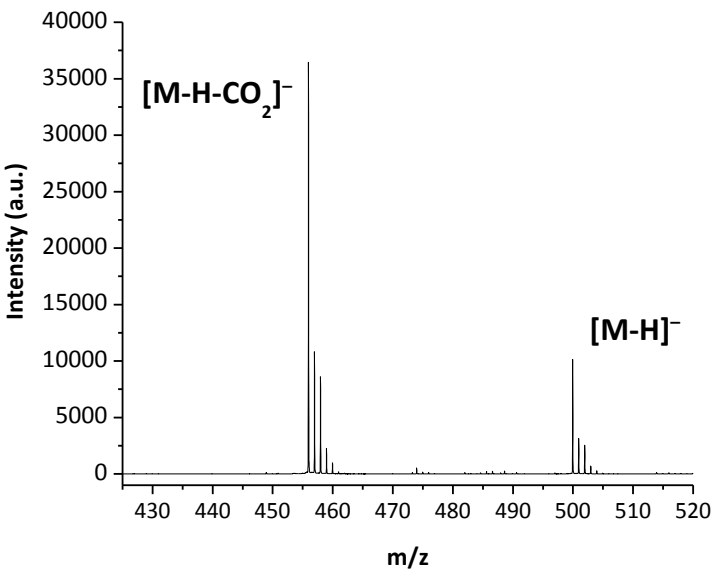

Figure 6S. HR-MS (ESI) spectrogram of **DTB-T**.

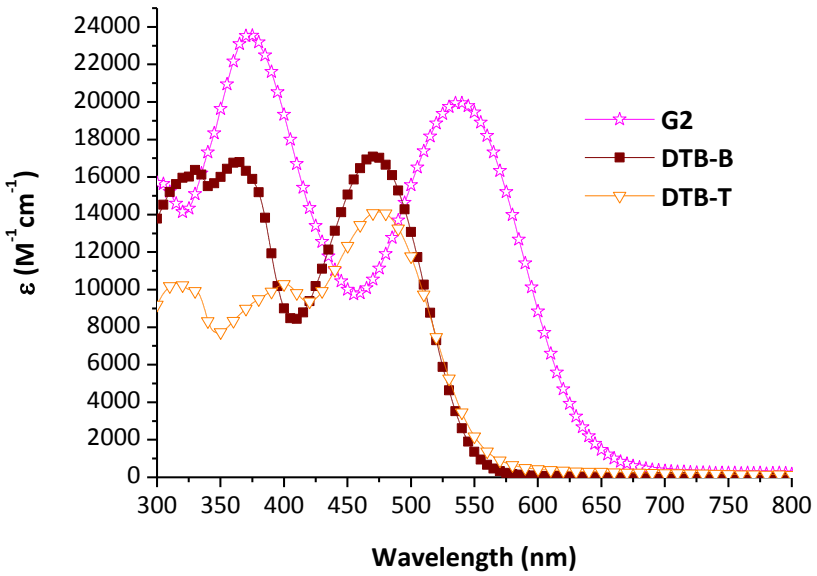

Figure 7S. Absorption spectra of **G2**, **DTB-B** and **DTB-T** recorded in THF.

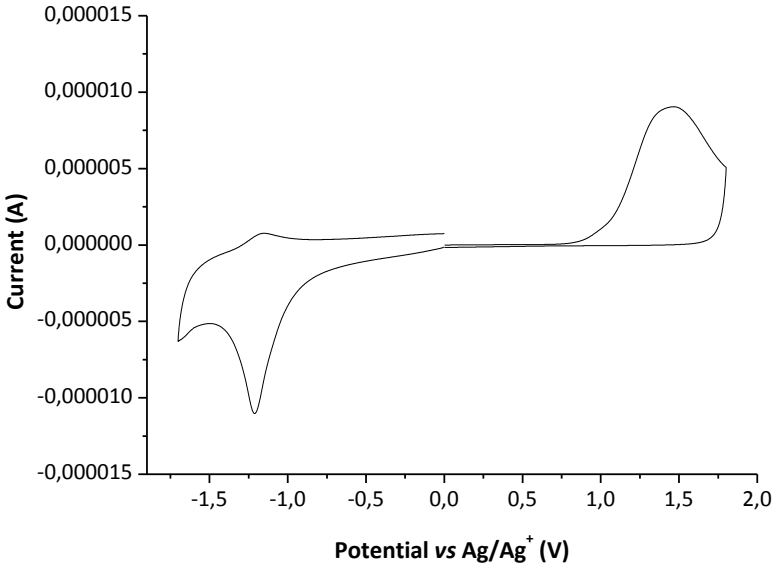

Figure 8S. Cyclic voltammogram of **DTB-B**.

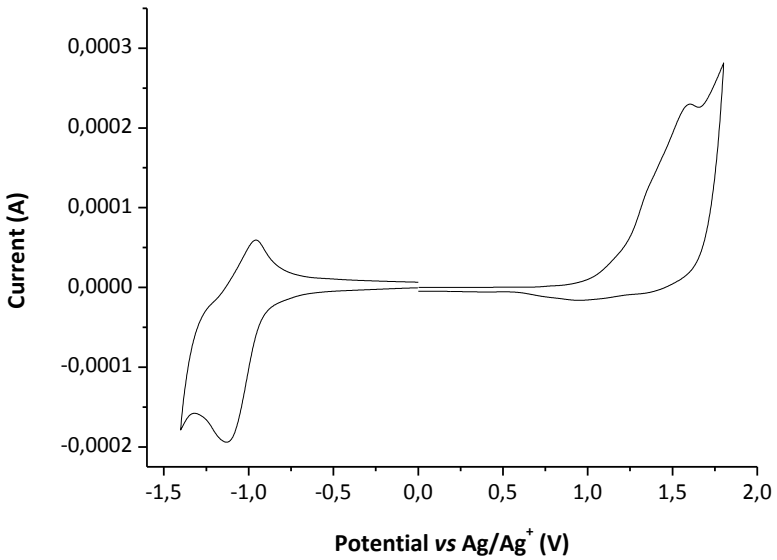

Figure 9S. Cyclic voltammogram of **DTB-T**.

Device fabrication and characterization: Fluorine-doped tin oxide (FTO, 10 Ω/sq, provided by Solaronix S.A.) glass plates were cleaned in a detergent solution using an ultrasonic bath for 15 min and subsequently rinsed with water and ethanol. Double-layer photo-anodes (thickness 17 μm) were prepared as follows: *i*) a layer of commercial colloidal paste (Dyesol 18NR-T) was deposited onto the FTO glass and dried at 125°C for 15 min to obtain a transparent nano-crystalline film (~12 μm); *ii*) a scattering layer (~5 μm, Solaronix D/SP colloidal paste) was deposited onto the transparent layer; *iii*) a sintering process was performed at 450°C for 30 min. The thickness and the active area (0.16 cm^2) of the sintered photo-anodes was measured using a profilometer (Tencor Alpha-Step 500 Surface Profiler). The dye loading was performed by immersing the photoanodes in 0.2 mM THF solutions of the individual dyes (**G2, DTB-B** or **DTB-T** for devices A, B and C, respectively) containing chenodeoxycholic acid (CDCA, 10 mM) and kept for 14 h in dark at room temperature. The co-sensitized photo-anodes were prepared by dyeing them into appropriate solutions of **G2** (0.1 mM) and **DTB-B** (0.05 mM, device D) or **DTB-T** (0.05 mM, device E) in THF containing CDCA (10 mM). The counter-electrodes were prepared by sputtering a 50 nm Pt layer on a suitably cleaned FTO plate. The two electrodes were faced and assembled by means of a gasket of 50 mm-thick Surlyn® foil (Dyesol Ltd) interposed between them. The redox electrolyte (0.1 M LiI, 0.02 M I_2, 0.6 M 1-methyl-3-propylimidazolium iodide, and 0.5 M *tert*-butylpyridine in dry acetonitrile) was vacuum-injected into the space between the electrodes through holes suitably pre-drilled through the counter-electrodes.

The surface concentrations (dye loading) of the dyes were assessed by spectrophotometric determination as follows: double layered photoanodes (12 + 5 μm, 1 cm^2) were sensitized with the same solutions used for devices A-E; then the dyes were completely desorbed from the TiO_2 surface by immersing the substrates in a 0.01 M tetrabutylammonium hydroxide in DMF solution (20 ml). The molar concentration of each dye was estimated by the Lambert-Beer's low from the absorption spectra of the resulting desorption solutions taking into account the molar extinction coefficient of the individual dyes at the corresponding λ_{max}.

Photocurrent-voltage measurements were performed using a Keithley Model 2400 Source Meter. A Newport 91160A AM 1.5 Solar Simulator equipped with a 1000W xenon arc lamp served as a light source. The light intensity (or radiant power) was calibrated to 100 $mWcm^{-2}$ using as reference a Si solar cell. A mask (0.25 cm^2 aperture) was applied to the devices before the measurements. The incident photon-to-current conversion efficiency (IPCE) was measured by the DC method. IPCE measurements were carried out with a computerized setup consisting of a xenon arc lamp (140 W, Newport, 67005) coupled to a Cornerstone 260 Oriel 74125 monochromator. Light intensity was measured by a calibrated UV silicon

photodetector (Oriel 71675) and the short-circuit currents were measured by using a Newport 2936-C dual-channel optical power/energy meter.

Electrochemical impedance spectroscopy (EIS) was performed using a Metrohm Autolab PGSTAT 302N (Eco Chemie B.V.) potentiostat in a frequency range between 100 kHz and 10 mHz. The impedance measurements were carried out at different voltage biases under 1.0 sun illumination. The resulting impedance spectra were fitted with the ZView software (Scribner Associates). EIS spectra were analyzed through the well-known equivalent circuit. All electrochemical parameters have been plotted as a function of the corrected potential in order to take into account the losses due to the total series resistance, which lead to a potential drop, that is not associated with the displacement of the Fermi level.

Mixture of dyes	○ □[%]	○ V_{OC} [V]	FF	○ J_{SC} [mA/cm^2]
G2/DTB-B (3:1)	**5.9**	0.70	0.66	12.8
G2/DTB-B (2:1)	**6.2**	0.67	0.67	13.9
G2/DTB-B (1:1)	**5.7**	0.68	0.67	12.5
G2/DTB-T (3:1)	**6.8**	0.69	0.70	14.1
G2/DTB-T (2:1)	**7.8**	0.71	0.72	15.3
G2/DTB-T (1:1)	**6.6**	0.71	0.68	13.7
G2/DTB-T (1:2)	**5.4**	0.72	0.67	11.1
G2/DTB-T (1:3)	**3.6**	0.82	0.65	6.8

Table 1S. Photovoltaic parameters of devices based on different dye mixtures measured under 1.0 sun illumination (AM 1.5, 100 mW/cm^2).

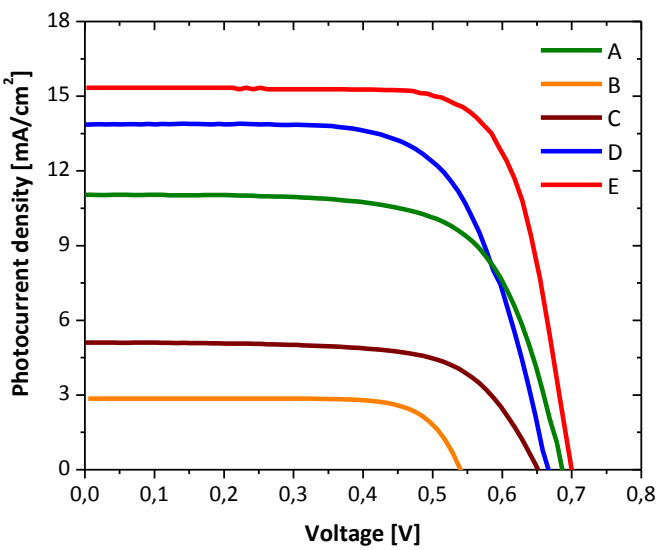

Figure 10S. J-V curves for devices A-E.